

## Article

# The Influence of Copper Content on the Elastic Modulus and Antibacterial Properties of Ti-13Nb-13Zr-xCu Alloy

Xinru Mao <sup>1</sup>, Anqi Shi <sup>1</sup>, Renxian Wang <sup>2</sup>, Jingjun Nie <sup>2</sup>, Gaowu Qin <sup>1,3</sup>, Dafu Chen <sup>2,\*</sup> and Erlin Zhang <sup>1,3,\*</sup>

- <sup>1</sup> Key Laboratory for Anisotropy and Texture of Materials, Education Ministry of China, School of Materials Science and Engineering, Northeastern University, Shenyang 110819, China; xinru\_mao@126.com (X.M.); shianqi919@126.com (A.S.); qingw@mail.neu.edu.cn (G.Q.)
- <sup>2</sup> Laboratory of Bone Tissue Engineering, Beijing Laboratory of Biomedical Materials, Beijing Research Institute of Orthopaedics and Traumatology, Beijing Jishuitan Hospital, Beijing 100035, China; wrxpumc@126.com (R.W.); niejingjun\_jst@126.com (J.N.)
- <sup>3</sup> Research Center for Metallic Wires, Northeastern University, Shenyang 110819, China
- \* Correspondence: chendafu@jsthospital.org (D.C.); zhangel@atm.neu.edu.cn (E.Z.); Tel./Fax: +86-24-8368-9400 (E.Z.)

**Abstract:** Device-related infection or inflammatory and stress shield are still the main problems faced by titanium alloy implants for long-term implantation application; therefore, it is of great significance to design an alloy with low elastic modulus and good antibacterial properties as well as good biocompatibility. In this paper, Ti-13Nb-13Zr-xCu (x = 3, 7 wt.%) alloys were designed and prepared to reveal the influence of Cu content on the elastic modulus and antibacterial property. X-ray diffractometer, metallographic microscope, scanning electron microscope, and transmission electron microscope were used to study the phase transformation, microstructure, mechanical properties, antibacterial properties, and cytotoxicity of the alloys. The experimental results have demonstrated that the antibacterial performance and the elastic modulus were significantly improved but the corrosion resistance deteriorated with the increase of the copper content. Ti-13Nb-13Zr-3Cu with a low modulus of 73 GPa and an antibacterial rate of over 90% against *Staphylococcus aureus* (*S. aureus*) exhibited great potential as a candidate for implant titanium in the future.

**Keywords:** Ti-13Nb-13Zr; microstructure; cytotoxicity; Cu-containing titanium alloy; antibacterial property



**Citation:** Mao, X.; Shi, A.; Wang, R.; Nie, J.; Qin, G.; Chen, D.; Zhang, E. The Influence of Copper Content on the Elastic Modulus and Antibacterial Properties of Ti-13Nb-13Zr-xCu Alloy. *Metals* **2022**, *12*, 1132. <https://doi.org/10.3390/met12071132>

Academic Editor: Antonio Riveiro

Received: 24 May 2022

Accepted: 28 June 2022

Published: 1 July 2022

**Publisher's Note:** MDPI stays neutral with regard to jurisdictional claims in published maps and institutional affiliations.



**Copyright:** © 2022 by the authors. Licensee MDPI, Basel, Switzerland. This article is an open access article distributed under the terms and conditions of the Creative Commons Attribution (CC BY) license (<https://creativecommons.org/licenses/by/4.0/>).

## 1. Introduction

Titanium has excellent corrosion resistance, biocompatibility, and high specific strength, which is of great significance in the field of biomedical metal materials [1]; therefore, it has been widely applied in clinical operation and medical equipment. However, as implanted devices, titanium implants still face such problems as postoperative bacterial infection and inflammatory response [2]. In addition, the mismatch in the elastic modulus between bio-implants and human bone causes stress shielding effects, osteoporosis, implant loosening, and even implant failure [3].

Previous studies have shown the elastic modulus of a titanium alloy can be regulated by adjusting the composition of major alloying elements such as Nb, Zr. For example, the elastic modulus of Ti-13Nb-13Zr (named TNZ) alloy was as low as (65–82) GPa depending on the heat treatment history [4]. D. Kuroda et al. [5] successfully designed and developed quaternary  $\beta$ -type titanium alloys with an elastic modulus of as low as about 50 GPa using molecular orbital calculation methods based on electronic structures, including Ti-Nb-Zr-Ta and Ti-Nb-Ta-Sn alloy systems.

On the other hand, some researchers have shown that adding Cu and Ag to titanium alloys can improve their antibacterial properties [6]. Shirai et al. first confirmed that the addition of 1% copper made the antibacterial capacity of the alloy up to 80% and the

antibacterial activity was unstable when 2 wt.% copper was added to titanium alloy [7]. Ma et al. [8] proved Ti-5Cu alloy had a good inhibitory effect on *Staphylococcus aureus* (*S. aureus*), and the inhibitory rate reached 92.7%. Zhang et al. proved Ti-Cu sintered alloys had good antibacterial effect when the Cu ion release concentration was higher than 0.34 mg/L [9].

More recently, Cu or Ag was introduced into  $\beta$  or near  $\beta$  titanium in order to obtain a new titanium alloy with low modulus and good antibacterial performance. Shi et al. [10] reported the addition of 5 wt.% Cu clearly improved the antibacterial effect of Ti-13Nb-13Zr-5Cu (92.7% reduction); however, the elastic modulus of the alloy was increased from 65 GPa to 82 GPa because of the precipitation of  $Ti_2Cu$  phase and  $\alpha''$  phase. Cai et al. [11] found that antibacterial rate of TNZ was improved to 98% by adding 13 wt.% Ag, but the presence of  $Ti_2Ag$  phase and  $\alpha$  phase also increased the elastic modulus from 75 GPa to 82 GPa.

According to the previous results, the precipitation of  $Ti_2Cu$  phase contributed significantly to the antibacterial performance of Ti-Cu alloy [12] and the antibacterial effect increased with the increase in  $Ti_2Cu$  phase fraction [9]. Yet the precipitation of  $Ti_2Cu$  phase also accelerated the phase transition process:  $\beta \rightarrow \alpha + Ti_2Cu$ . Because of the high elastic modulus of  $\alpha$  phase and  $Ti_2Cu$  phase, therefore, the addition of antibacterial element Cu and the strict adjustment of the phase composition are the key factors to obtain low modulus and antibacterial titanium alloy.

Figure 1 is a three-dimensional diagram of the elastic modulus of some titanium alloys according to the Bond order ( $\overline{Bo}$ )/Metal d-orbital energy ( $\overline{Md}$ ) diagram of titanium alloys [13,14]. On the basis of the calculation formula of  $\overline{Md}$  and  $\overline{Bo}$  values in molecular orbital calculation of DV- $X\alpha$ Cluster [11]:

$$\overline{Md} = \sum_i^n Xi(Md)_i \quad (1)$$

$$\overline{Bo} = \sum_i^n Xi(Bo)_i \quad (2)$$

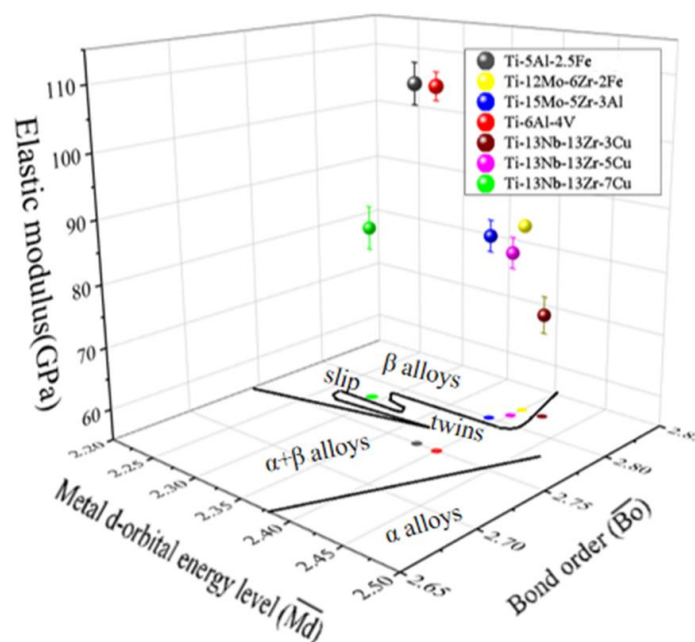


**Figure 1.** Three-dimensional diagram of ( $\overline{Bo}$ )-( $\overline{Md}$ ) and elastic modulus trend prediction of titanium alloy [10,13,14].

The calculated  $\overline{Md} = 2.42$ ,  $\overline{Bo} = 2.82$  of TNZ-3Cu alloy and  $\overline{Md} = 2.29$ ,  $\overline{Bo} = 2.77$  of TNZ-7Cu alloy were shown in Figure 1. The elastic modulus of Ti-13Nb-13Zr-xCu ( $x = 3, 7$ ) alloys are approximately (74–88) GPa, indicating that titanium alloys with low modulus can be obtained by adding copper.

Previous results have shown the antibacterial properties of copper-bearing titanium alloys were closely related to the Cu content. For example, the antibacterial rate was 92.5% for Ti-3Cu in comparison with cp-Ti, and 99.4% for Ti-5Cu and 99.9% for Ti-7Cu, respectively [15]. Although high Cu content enhanced the antibacterial ability, it did not improve the corrosion resistance of the alloy, and might affect the strength-plasticity as well as cytotoxicity [3]. In titanium copper binary phase diagram, when the mass fraction of Cu is about 7% or high, the eutectoid structure will be formed [16], which could improve the strength but worsen the plasticity.

In view of the above considerations, the Cu content in TNZ alloy was designed to be 3% and 7% in this study, respectively. The influence of Cu content was investigated on the microstructure, elastic modulus, corrosion resistance, antibacterial properties, and biocompatibility. The preliminary results have shown TNZ-3Cu alloy exhibited a modulus of 73 GPa and good antibacterial rate of >90% against *S. aureus* as well as good biocompatibility. The lower elastic modulus and the stronger antibacterial properties of TNZ-3Cu in comparison with cp-Ti and Ti-6Al-4V alloy suggested that this alloy could reduce the stress shield effect and the device-related inflammation and might be a candidate for titanium alloy in the future.

## 2. Experimental

### 2.1. Preparation of Materials

Titanium sponge for industry (99.9 wt.%), sponge zirconium (99.9 wt.%), copper (99.99 wt.%), and Ti-50Nb (wt.%) master alloy were used to prepare Ti-13Nb-13Zr-xCu (wt.%,  $x = 3$  and 7, named TNZ-3Cu and TNZ-7Cu, respectively). The two alloys were melted for at least 6 times in a high vacuum non-consumable arc melting furnace to obtain alloy ingots.

Samples with a size of  $\Phi 15$  mm  $\times$  2 mm and 48 mm  $\times$  10 mm  $\times$  2 mm were cut from the titanium ingots, vacuum solid solution treated at 950 °C for 4 h before water quenching (named T4). Then, the samples were vacuum aged at 600 °C for 15 min (named T6-15m), 30 min (named T6-30m), 1 h (named T6-1h), and 2 h (named T6-2h), respectively, and cooled down to room temperature in air. After this, the samples were ground with up to 2000# silicon carbide sandpaper, and polished by diamond polishing solution (Shenzhen Nanos Precision Machinery Technology, Shenzhen, China) and cleaned finally with acetone (Tianjin Fuyu Fine Chemicals, Tianjin, China), anhydrous ethanol (Tianjin Fuyu Fine Chemicals, Tianjin, China), and ultrapure water.

### 2.2. Microstructure Observation

Samples were etched with Kroll solution (HF:HNO<sub>3</sub>:H<sub>2</sub>O = 2:5:50) (Sinopharm Chemical Reagent, Shenyang, China). A metallographic microscope (OLYMPUS GX71, Tokyo, Japan), a JSM6360LV scanning electron microscope (SEM) (JEOL Corporation of Japan, Tokyo, Japan) with energy dispersive X-ray spectrometer (EDS) (ULTRA PLUS, Zeiss group, Oberkochen, Germany), and a transmission electron microscope (TEM) (EOL JEM-2100F, JEOL Corporation of Japan, Tokyo, Japan) were applied to metallographic microstructure and chemical composition analysis according to the normal preparation procedure.

### 2.3. Hardness and Elastic Modulus

According to the national standard (GB/T 31544-2015), the sample with a size of 48 mm  $\times$  10 mm  $\times$  2 mm was applied to the elastic modulus test on a solid material dynamic performance tester (China Building Materials Testing and Certification Center,

Shenyang, China). The mean and standard deviation are obtained from three ordinary patterns. The calculation formula of elastic modulus(E) is as follows:

$$E = 0.9465 \frac{mf_r^2}{b} \left(\frac{L}{t}\right)^3 \left[1 + 6.585\left(\frac{t}{L}\right)^2\right] \quad (3)$$

where, m—sample mass, kg;  $f_r$ —Response frequency of foundation bending, Hz; b—sample width, m; L—sample length, m; t—sample thickness, m.

Vickers microhardness was measured by 401MVDTM Vickers hardness tester (Dongguan Shenghong Testing Instrument, Dongguan, China). A 200 g load was applied and the load duration was set to 15 s. Twelve random points were selected to get the mean with standard deviation.

#### 2.4. Electrochemical Test

The corrosion properties were tested on a Versa STAT V3-400 electrochemical workstation (Ametek Trading, Shanghai, China). The sample was embedded in the mold and placed in SBF solution (NaCl: 8 g/L; KCl: 0.4 g/L; NaHCO<sub>3</sub>: 0.35 g/L; CaCl<sub>2</sub>: 0.14 g/L; MgSO<sub>4</sub>: 0.2 g/L; Na<sub>2</sub>HPO<sub>4</sub>: 0.12 g/L; KH<sub>2</sub>PO<sub>4</sub>: 0.06 g/L) at (37 ± 0.5) °C [17]. In a standard three-electrode configuration, saturated calomel was used as a reference electrode, platinum as a counter electrode, and the sample as a working electrode. According to ISO 10271:2001 standard, the potentiodynamic polarization curve (Tafel) was tested at a scanning rate of 0.5 mV/s in the range of −0.15 V to 0.75 V. To ensure the reliability of the experimental results, at least three parallel samples were selected.

#### 2.5. Ion Release

The sample was soaked in 3.5 mL 0.9% NaCl (Sichuan Kelun Pharmaceutical, Chengdu, China) solution, and the Cu ion release concentration was determined at day 1, 3, 7 and 15. Three parallel samples were selected for every group. and the concentration of Cu ion was determined by Agilent ICP-7700 ion detector (Perkin Elmer Inc, Shanghai, China), and the average value was taken.

#### 2.6. Antibacterial Properties

*Staphylococcus aureus* (*S. aureus*, ATCC6538) was chosen to test the antibacterial performance of the samples. cp-Ti was chosen as the control group. The samples were placed in a 12-well plate. 100 µL bacterial suspension with a concentration of 10<sup>5</sup> cfu/mL was dropped on each sample and then cultured in a dark and humid incubator at 37 °C for 24 h. Then, the sample was cleaned with 2 mL sterile saline (Sichuan Kelun Pharmaceutical, Chengdu, China) and oscillated in a vortex oscillator for 1 min to ensure the bacteria on the sample surface were oscillated off. Then, 100 µL of the washing solution was inoculated on nutrient medium for 24 h. Finally, bacterial colony number was counted referring to national standard GB/T 4789.2-2010. The following formula was used to calculate antibacterial rate(AR):

$$AR = \frac{N_{\text{control}} - N_{\text{sample}}}{N_{\text{sample}}} \times 100\% \quad (4)$$

where,  $N_{\text{control}}$  and  $N_{\text{sample}}$  represent the average number of bacteria on cp-Ti and TNZ-xCu samples, respectively [18]. According to the National Standard of China (GB/T 4789.2-2010),  $AR \geq 99\%$  reveals the sample has strong antibacterial performance, and  $AR \geq 99\%$  reveals the sample has antibacterial performance.

#### 2.7. Live/Dead Staining

Bacterial survival was assessed on the samples using live/dead staining techniques. Live/Dead BacLight™ bacterial viability kit (L13152, Shanghai Biyuntian Biotechnology, Shanghai, China) was used according to the instruction. SYTO-9 and propidium iodide (PI) were used in the experiment, which are evenly mixed with 5 mL deionized water.

The red fluorescent Pi was identified as dying cells with damaged membranes, while intact bacterial cells were colored green.

### 2.8. Morphology of the Bacteria

The bacteria cultured at 37 °C for 24 h were taken out, the bacteria and metabolites of the sample were washed with normal saline. Then the samples were fixed for at least 2 h with 2.5% glutaraldehyde solution (Sinopharm Chemical Reagent, Shenyang, China). After the fixation, the glutaraldehyde solution was sucked, and the sample was dehydrated by 30%, 50%, 70%, 90%, and 100% ethanol, dried in an oven (DHP-360, Beijing Yongguangming Medical Instrument, Beijing, China), and then gold sprayed. Finally, the morphology and distribution of bacteria on the sample surface was observed under SEM.

### 2.9. Cytotoxicity

MC3T3-E1 cell (Cell Resource Center, Shanghai Institute of Life Sciences, Shanghai, China) was selected to assess cytotoxicity. cp-Ti and TNZ-xCu (wt.%, x = 3, 7) samples aged at 600 °C for 2 h were selected for the cytotoxicity assessment. During the experiment, the sample was immersed in minimum Eagle's medium (MEM, volume 3.5 mL) (Thermo Fisher Technologies LTD, Shanghai, China) at 37 °C for three days to prepare the extract. The cell inoculation density was  $2 \times 10^4$  cells/mL, and the medium was changed every 48 h. The extracts and the cells were cultured at 37 °C and 5% CO<sub>2</sub>, at the preset time (1 day, 3 days and 7 days), and 10 µL 10% CCK-8 solution was added. After 4 h of cultivation, the CCK-8 (Shanghai Biyuntian Biotechnology, Shanghai, China) was siphoned out, and 100 µL DMSO (Sinopharm Chemical Reagent, Shenyang, China) solution was added to every well to make the solution color. After we shook the solution for 15 min, the optical density (OD) was detected at 450 nm by a microplate reader (iMark, Bole Company, Shenyang, China). Finally, the morphology and distribution of cells on the sample surface were observed under SEM.

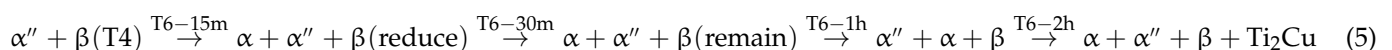
### 2.10. Statistical Analysis

All experiments were repeated three times, with mean  $\pm$  standard deviation representing representative results, which were quantitatively and statistically analyzed by *t*-test; *p* < 0.05 was considered statistically to be significant.

## 3. Results

### 3.1. Phase Constitution

Figure 2a shows XRD patterns of TNZ-3Cu samples. At T4 state, only  $\beta$  and  $\alpha''$  phases were detected in TNZ-3Cu, indicating the alloy was mainly composed of  $\beta$  and  $\alpha''$  phases at high temperature. When the aging treatment lasted for 15 min, the peak of  $\beta$  phase at  $2\theta = 38^\circ$  disappeared, while peaks of  $\alpha$  phase at  $2\theta = 39^\circ$  and Ti<sub>2</sub>Cu at  $2\theta = 62.5^\circ$  were detected, showing that Ti<sub>2</sub>Cu phase precipitated and  $\alpha$  phase was formed. Since the diffraction peak of  $\alpha$  phase coincides with that of Ti<sub>2</sub>Cu, the existence and relative content of  $\alpha$  phase cannot be determined by XRD results. When the aging time was 30 min,  $\beta$  phase at  $2\theta = 38^\circ$  reappeared. After the aging treatment for 1 h, a new diffraction peak of  $\beta$  phase appeared at  $2\theta = 55^\circ$ , and  $\alpha$  phase at  $2\theta = 52^\circ$  was detected. With the aging time extended to 2 h, a new diffraction peak of Ti<sub>2</sub>Cu phase was detected at  $2\theta = 42^\circ$ . The above results indicated that the following phase transition processes occurred in TNZ-3Cu alloy during the aging treatment:



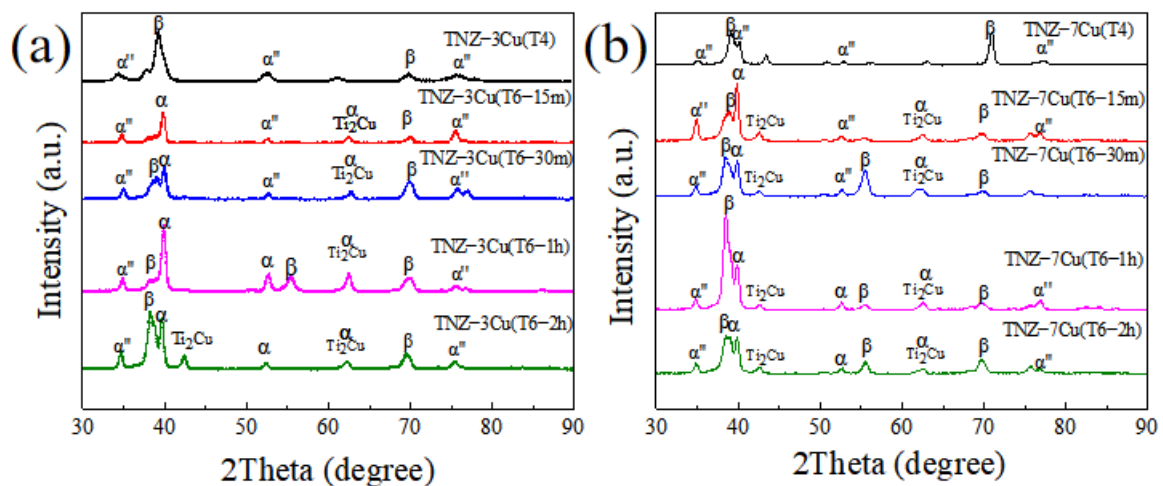


**Figure 2.** XRD patterns of TNZ-xCu (wt.%,  $x = 3, 7$ ) after different heat treatments (a) TNZ-3Cu; (b) TNZ-7Cu.

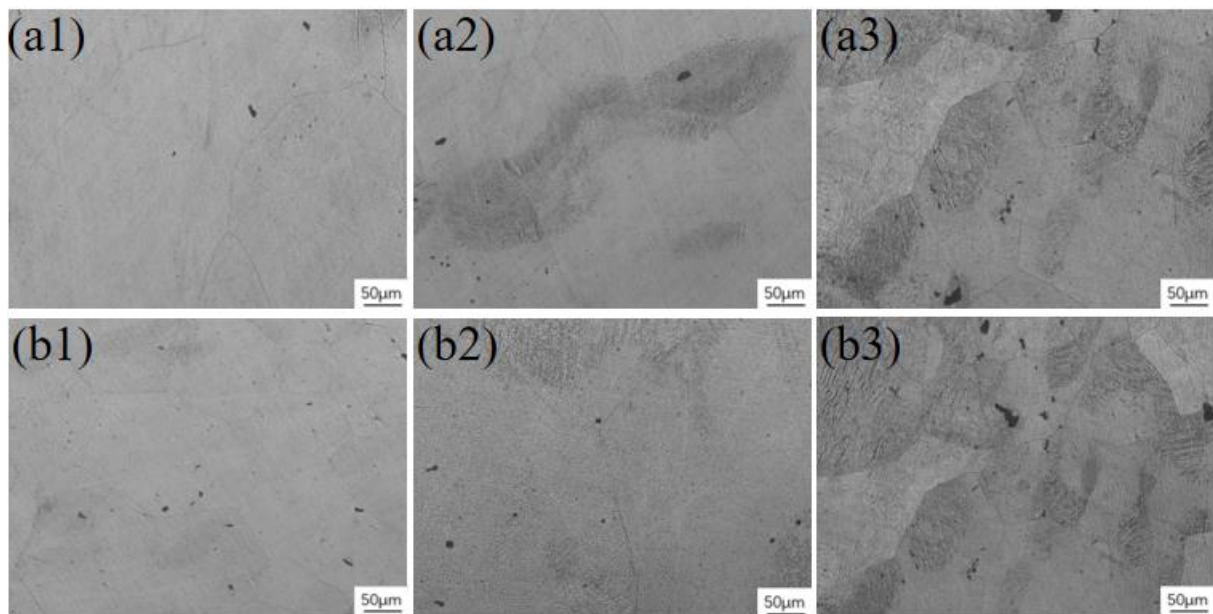
Figure 2b shows XRD pattern of TNZ-7Cu samples. TNZ-7Cu(T4) alloy was mainly composed of  $\beta$  phase and  $\alpha''$  phase, similar to TNZ-3Cu(T4) alloy. After 15 min of aging, the diffraction peak of  $Ti_2Cu$  appeared in TNZ-7Cu alloy while  $\beta$  phase at  $2\theta = 38^\circ$  was still detected. At 30 min, the diffraction intensity of  $\alpha''$  phase at  $2\theta = 35^\circ$  decreased while the diffraction intensity of  $\beta$  phase at  $2\theta = 38^\circ$  and  $2\theta = 55^\circ$  increased. At 1 h, the diffraction peak of  $\beta$  phase at  $2\theta = 38^\circ$  was further enhanced. However, in TNZ-7Cu(T6-2h) alloy, the diffraction intensity of  $\beta$  phase began to decrease. It is speculated that TNZ-7Cu(T6) alloy was mainly composed of  $\alpha$  phase,  $\beta$  phase, and  $Ti_2Cu$  phase.

### 3.2. Microstructure

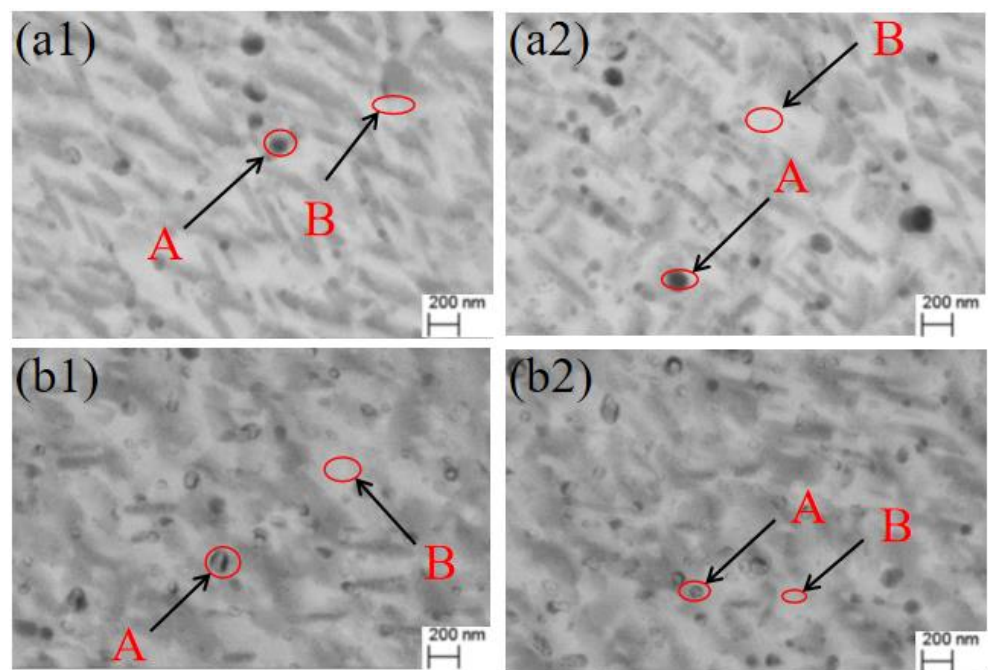
Figure 3 reveals the optical microstructure of TNZ-xCu alloys under different aging time. At T4 state, large  $\beta$  phase was observed in both alloys. At T6-30m state, the dark acicular phase was observed obviously near the grain boundary of  $\beta$  phase, and it is speculated that the acicular structure was composed of  $\alpha$  phase and  $\alpha''$  phase. After 2 h of aging treatment, more acicular phases were observed near the grain boundary. However, even after 2 h of aging treatment,  $Ti_2Cu$  precipitates could not be found under the optical microscope.

Figure 4 reveals the SEM microstructure of the alloys under different aging time. Three types of different phases can be seen in TNZ-3Cu(T6-30m), as shown in Figure 4(a1): gray acicular phase and black particles (Area A) in white matrix (Area B). After the aging treatment for 2 h, a similar microstructure was found, as shown in Figure 4(a2), the size and the morphology of the phases did not change obviously. Same microstructure and change tendency was also observed in TNZ-7Cu samples, as shown in Figure 4(b1,b2), but it was obvious that there were more black particles in TNZ-7Cu than in TNZ-3Cu.

The morphology and microstructure of TNZ-3Cu(T4), TNZ-3Cu(T6-30m) and TNZ-3Cu(T6-2h) samples were observed by TEM, as shown in Figure 5. From the diffraction spot analysis in Figure 5(a1,a2), it can be seen that TNZ-3Cu(T4) was primarily composed of a large number of  $\beta$  phases and a small number of acicular  $\alpha''$  phases. After the aging treatment, the microstructure of the alloy changed obviously, and a large number of obvious lath structure were found in the alloy, and the lath structure changed more and more obviously when the aging time extended from 30 min to 2 h. The microstructure analysis of TNZ-3Cu(T6-30m) and TNZ-3Cu(T6-2h) alloys by selected area diffraction (SAD) showed that  $\alpha$  phase and  $Ti_2Cu$  phase precipitated on the basis of the original  $\beta$  phase and  $\alpha''$  phase, as shown in Figure 5(b1,b2,c1,c2). When the aging time extended from 30 min to 2 h, more and more  $\beta$  and  $\alpha$  phase slate-like structures were formed, and more and more  $Ti_2Cu$  phase precipitated.



**Figure 3.** Metallographic microstructure of TNZ-xCu samples; (a1) TNZ-3Cu(T4); (a2) TNZ-3Cu(T6-30m); (a3) TNZ-3Cu(T6-2h); (b1) TNZ-7Cu(T4); (b2) TNZ-7Cu(T6-30m); (b3) TNZ-7Cu(T6-2h).



**Figure 4.** SEM microstructure of TNZ-xCu(T6); (a1) TNZ-3Cu(T6-30m); (a2) TNZ-3Cu (T6-2h); (b1) TNZ-7Cu(T6-30m); (b2) TNZ-7Cu (T6-2h).

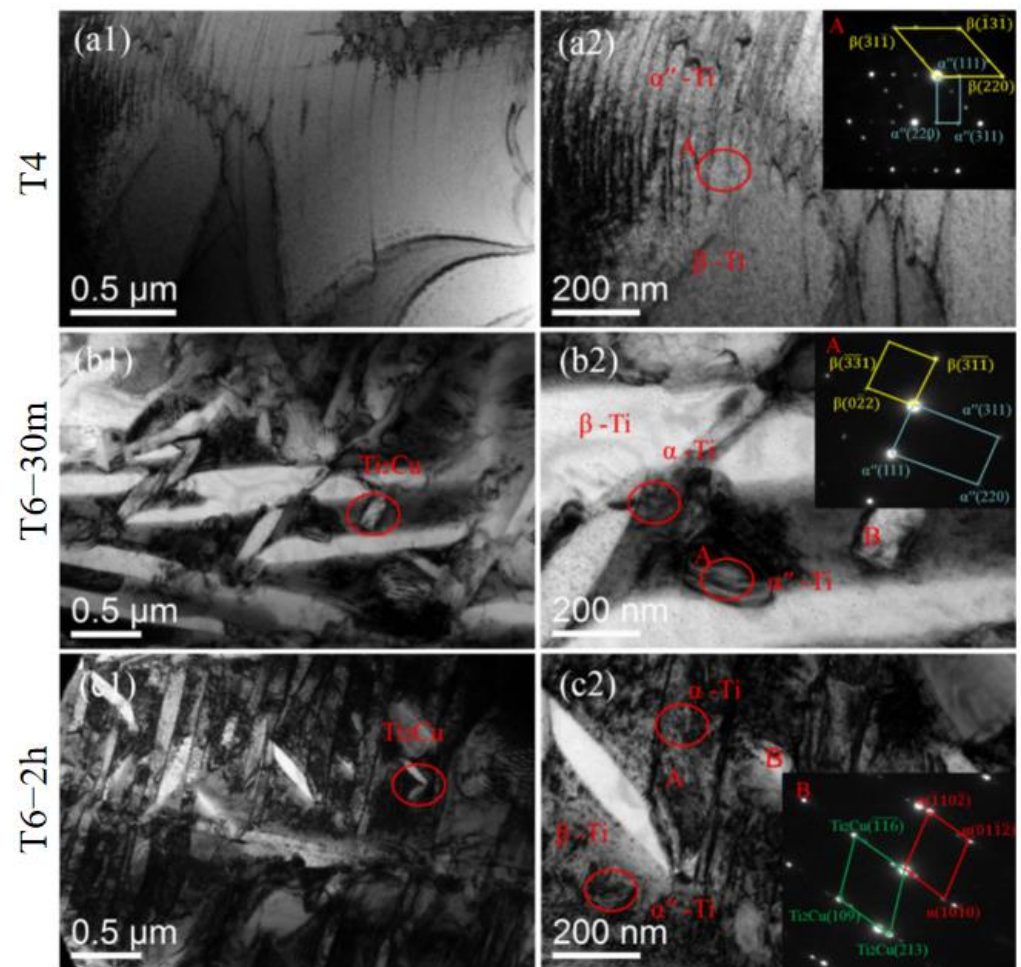


**Figure 5.** TEM images of TNZ-3Cu samples. (a1,a2) TNZ-3Cu(T4); (b1,b2) TNZ-3Cu(T6-30m); (c1,c2) TNZ-3Cu (T6-2h).

Similarly, the transmission structure analysis of TNZ-7Cu under the same heat treatment system is shown in Figure 6. TNZ-7Cu(T4) was composed of  $\beta$  phase and acicular  $\alpha''$  phase while TNZ-7Cu(T6-30m) and TNZ-7Cu(T6-2h) consisted of  $\beta$  phase,  $\alpha$  phase,  $\alpha''$  phase, and  $\text{Ti}_2\text{Cu}$  phase. Moreover, with the aging time extended from 30 min to 2 h, the net basket structure formed while  $\alpha$  phase and  $\beta$  phase increased, and  $\text{Ti}_2\text{Cu}$  particles also increased significantly. Table 1 summarizes the phase constitution of TNZ-xCu at different conditions.

**Table 1.** Phase constitution of TNZ-xCu at different conditions.

Alloys	T4	T6-15m	T6-30m	T6-1h	T6-2h
TNZ-3Cu	$\alpha'' + \beta$	$\alpha + \alpha'' + \beta$ (reduce)	$\alpha + \alpha'' + \beta$ (remain)	$\alpha + \alpha'' + \beta$	$\alpha + \alpha'' + \beta + \text{Ti}_2\text{Cu}$
TNZ-7Cu	$\alpha'' + \beta$	$\alpha + \alpha'' + \beta + \text{Ti}_2\text{Cu}$			

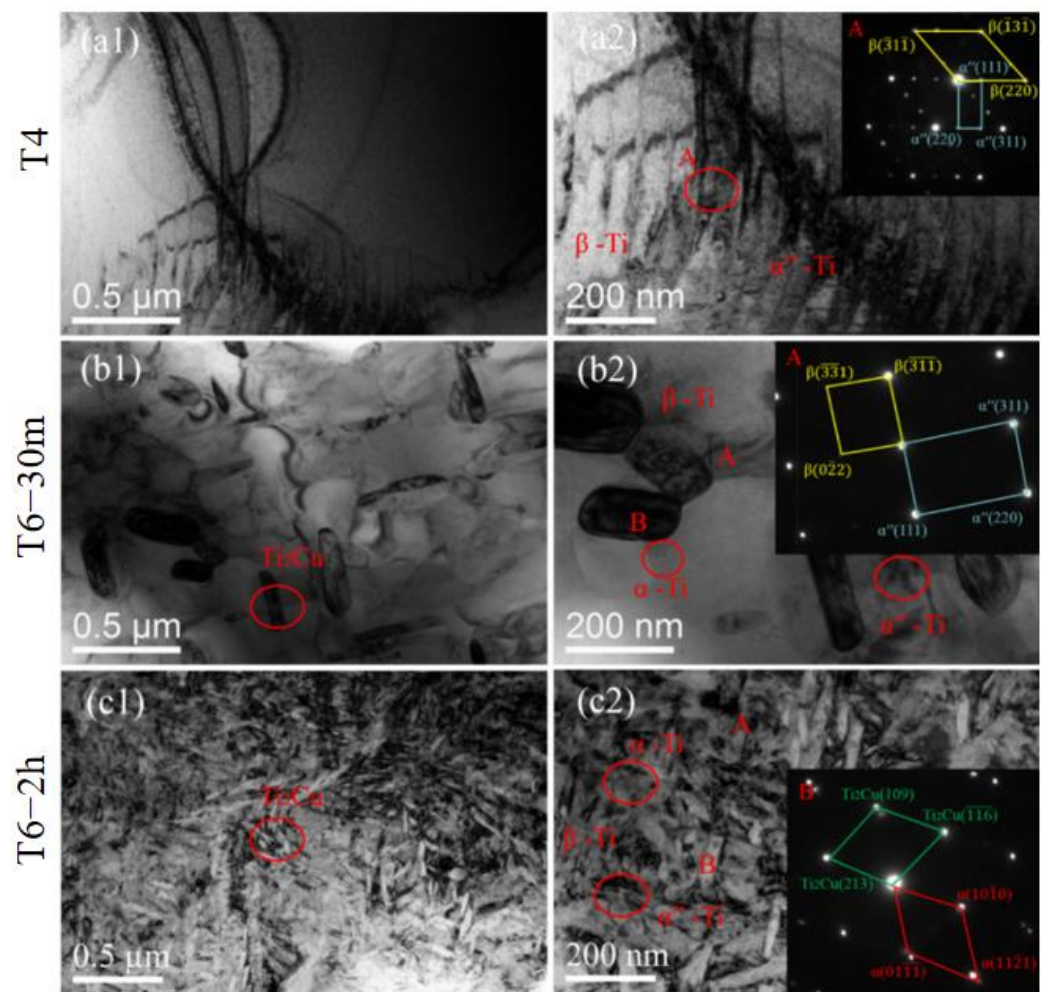


**Figure 6.** TEM images of TNZ-7Cu samples. (a1,a2) TNZ-7Cu(T4); (b1,b2) TNZ-7Cu(T6-30m); (c1,c2) TNZ-7Cu (T6-2h).

### 3.3. Microhardness

Figure 7a shows the microhardness of TNZ matrix alloy and TNZ-xCu (wt.%,  $x = 3, 7$ ) samples after T4 and T6 treatment. It can be found the addition of Cu increased the microhardness of TNZ alloy from 288HV to 340HV-346HV at T4 state, and high Cu content corresponded to a higher microhardness. For all alloys, the microhardness increased obviously with the extension of the aging treatment, and the hardness reached a relative stable value after 1 h aging treatment.

Figure 7b shows the elastic modulus of TNZ-xCu alloys, TNZ alloy, and traditional Ti-6Al-4V alloy. It can be found 3 wt.% Cu did not change the elastic modulus of TNZ alloy at T4 state, but 7 wt.% Cu increased the elastic modulus from 65 GPa to about 73 GPa. The elastic modulus increased significantly at the first 30 min to a stable value of 73 GPa for TNZ-3Cu and 84 GPa for TNZ-7Cu. Further aging treatment did not change the elastic modulus anymore.

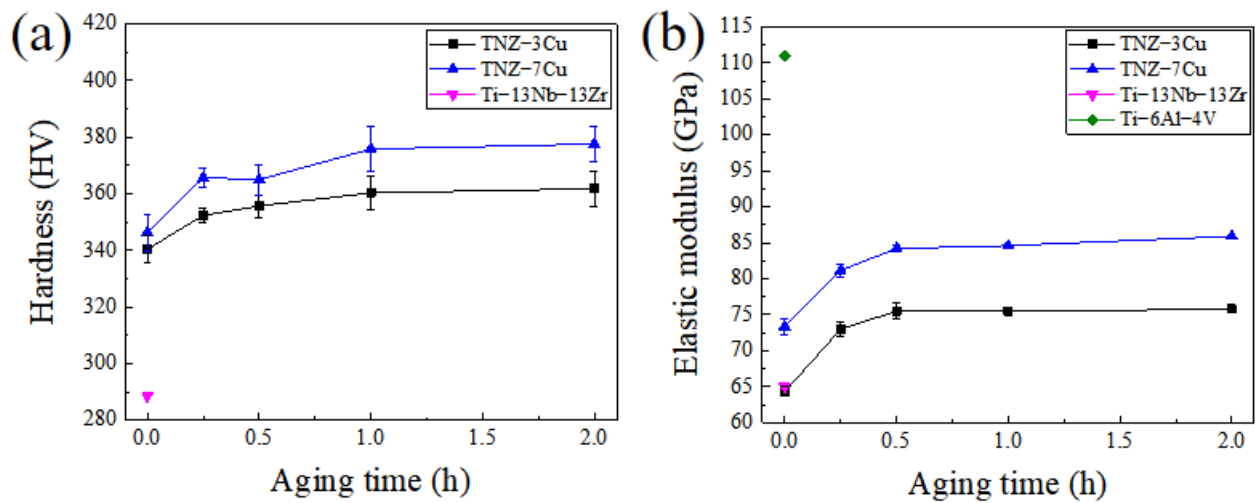


**Figure 7.** (a) Micro-vickers hardness and (b) elastic modulus of TNZ- $x$ Cu (wt.%,  $x = 3, 7$ ), and TNZ and Ti-6Al-4V alloys at different aging treatment conditions.

### 3.4. Corrosion Property

Figure 8a reveals the electrochemical results of cp-Ti, TNZ-3Cu and TNZ-7Cu samples. It can be found that the potential of all samples increased rapidly at first and then tended to be stable.  $E_{ocp}$  values obtained from open circuit potential (OCP) curves were listed in Table 2. By comparison, it is found that  $E_{ocp}$  value of TNZ-3Cu(T4) was more positive, but  $E_{ocp}$  of TNZ-7Cu(T4) was more negative than that of cp-Ti. The above results indicated the solid solution Cu element reduced the corrosion tendency but more Cu increased the corrosion tendency. The aging treatment reduced  $E_{ocp}$  value of TNZ-3Cu but increased  $E_{ocp}$  value of TNZ-7Cu, showing that the rapid formation of protective coatings in TNZ-7Cu due to the prolonged aging process.

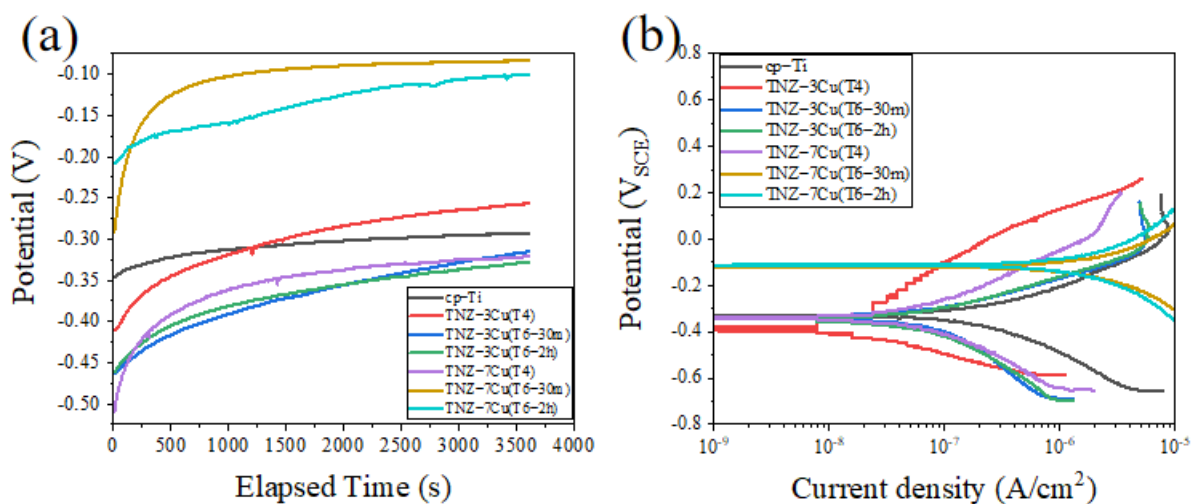


**Figure 8.** OCP curves and Tafel curves of TNZ- $x$ Cu (wt.%,  $x = 3, 7$ ) and cp-Ti; (a) OCP; (b) Tafel.

In the Tafel curve in Figure 8b, the aging treatment significantly moved the curve toward a more positive direction of the potential and high current density direction. More electrochemical parameters from Tafel were listed in Table 2. It can be found that TNZ-3Cu(T6) samples had slightly lower corrosion potential ( $E_{corr}$ ) and higher corrosion current density ( $i_{corr}$ ) than the TNZ-3Cu(T4) sample, which proved that aging treatment worsens corrosion resistance. Although the TNZ-7Cu(T4) sample had the same  $E_{corr}$  and  $i_{corr}$  as the TNZ-3Cu(T4) sample, the TNZ-7Cu(T6) sample exhibited much higher  $i_{corr}$  than TNZ-

7Cu(T4) and cp-Ti, indicating the corrosion resistance of the TNZ-7Cu alloy after aging treatment became worse.

**Table 2.** Electrochemical parameters of TNZ-xCu (wt.%, x = 3, 7) alloys and cp-Ti.

Samples	$E_{corr}$ (V)	$i_{corr}$ (A/cm <sup>2</sup> )	$E_{ocp}$ (V)
cp-Ti	$-0.327 \pm 0.019$	$(5.122 \pm 2.9) \times 10^{-8}$	$-0.297 \pm 0.029$
TNZ-3Cu(T4)	$-0.394 \pm 0.017$	$(1.102 \pm 2.3) \times 10^{-8}$	$-0.255 \pm 0.018$
TNZ-3Cu(T6-30m)	$-0.337 \pm 0.056$	$(1.787 \pm 4.1) \times 10^{-8}$	$-0.324 \pm 0.031$
TNZ-3Cu(T6-2h)	$-0.338 \pm 0.027$	$(1.494 \pm 5.5) \times 10^{-8}$	$-0.327 \pm 0.011$
TNZ-7Cu(T4)	$-0.340 \pm 0.029$	$(1.102 \pm 4.9) \times 10^{-8}$	$-0.320 \pm 0.019$
TNZ-7Cu(T6-30m)	$-0.119 \pm 0.019$	$(4.997 \pm 4.9) \times 10^{-7}$	$-0.095 \pm 0.016$
TNZ-7Cu(T6-2h)	$-0.114 \pm 0.031$	$(7.733 \pm 2.2) \times 10^{-7}$	$-0.104 \pm 0.019$

### 3.5. Cu Ion Dissolution

Figure 9 shows the Cu<sup>2+</sup> dissolution concentration and the dissolution rate of TNZ-3Cu(T6) and TNZ-7Cu(T6) samples in 0.9% NaCl solution up to 15 days. The concentration increased gradually while the dissolution rate decreased sharply with the extension of immersion. At all intervals, the sample with high Cu content showed a high dissolution process.

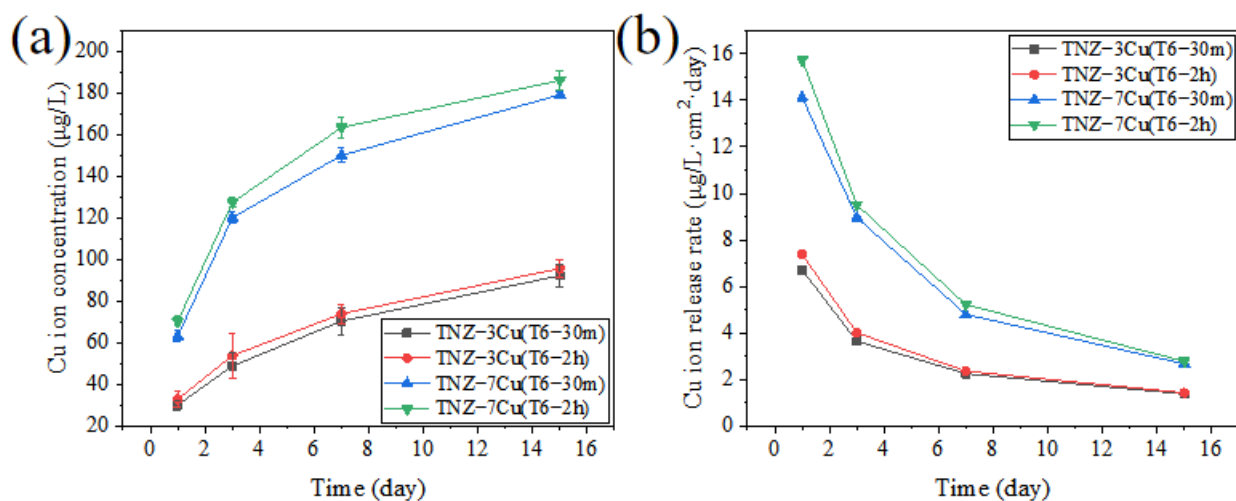


**Figure 9.** Cu ion accumulative release concentration and release rate from different TNZ-xCu(T6) alloys: (a) Cu ion release concentration, (b) Cu ion release rate.

### 3.6. Antibacterial Properties

Figure 10(a1–e1) shows *S. aureus* after 24 h in the co-culture of the control sample (cp-Ti) and TNZ-3Cu(T6). Large amount of colonies could be seen on cp-Ti, TNZ-3Cu(T6-15m), and TNZ-3Cu(T6-30m), indicating that cp-Ti did not show antibacterial properties, and short term aging treatment could not make the sample have antibacterial ability. It can be seen from Figure 10(d1–e1) that extending the aging time from 1 h to 2 h greatly reduced the number of bacteria in AGAR plate, indicating TNZ-3Cu(T6-1h) and TNZ-3Cu(T6-2h) samples had strong antibacterial performance.

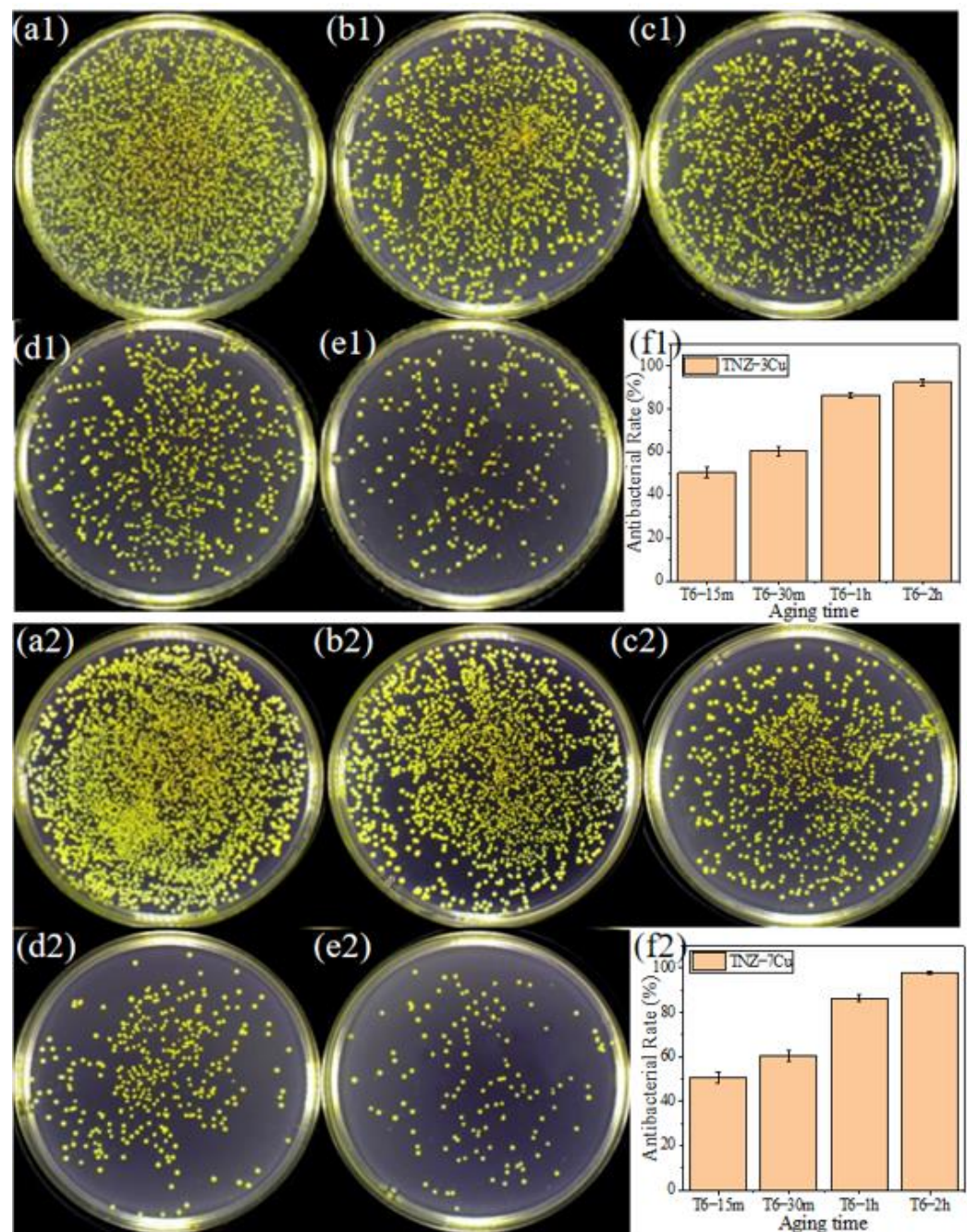


**Figure 10.** Typical bacteria colony cultured for 24 h on cp-Ti and TNZ-xCu (wt.%,  $x = 3,7$ ) samples and the antibacterial rate of different aging times. (a1,a2) cp-Ti; (b1,b2) T6-15m; (c1,c2) T6-30m; (d1,d2) T6-1h; (e1,e2) T6-2h; (b1–e1)TNZ-3Cu; (b2–e2) TNZ-7Cu; (f1,f2): the calculated antibacterial rate of TNZ-3Cu(T6) and TNZ-7Cu(T6).

A similar situation was observed in the case of TNZ-7Cu, as shown in Figure 10(a2–e2). Figure 10(f1,f2) show the calculated antibacterial rate of TNZ-3(T6) and TNZ-7Cu(T6) samples. The antibacterial rate increased with the extension of the aging time for both alloys and reached >90% after 2h aging treatment. At all intervals, TNZ-7Cu(T6) exhibited better antibacterial performance than TNZ-3Cu(T6).

Figure 11 illustrates the live and dead staining of *S. aureus* on different samples. A large amount of bacteria with green color were observed on the surface of cp-Ti samples, indicating the bacteria were live on good growth condition. These results demonstrated that cp-Ti basically has no antibacterial ability. Bacteria with green color and red color were

found on TNZ-xCu(T6-30m) samples, showing that some bacteria were dead. However, many dead bacteria and a few living bacteria were observed on TNZ-xCu(T6-2h) samples, indicating the antibacterial ability of the samples was significantly improved with the aging process from 30 m to 2 h.

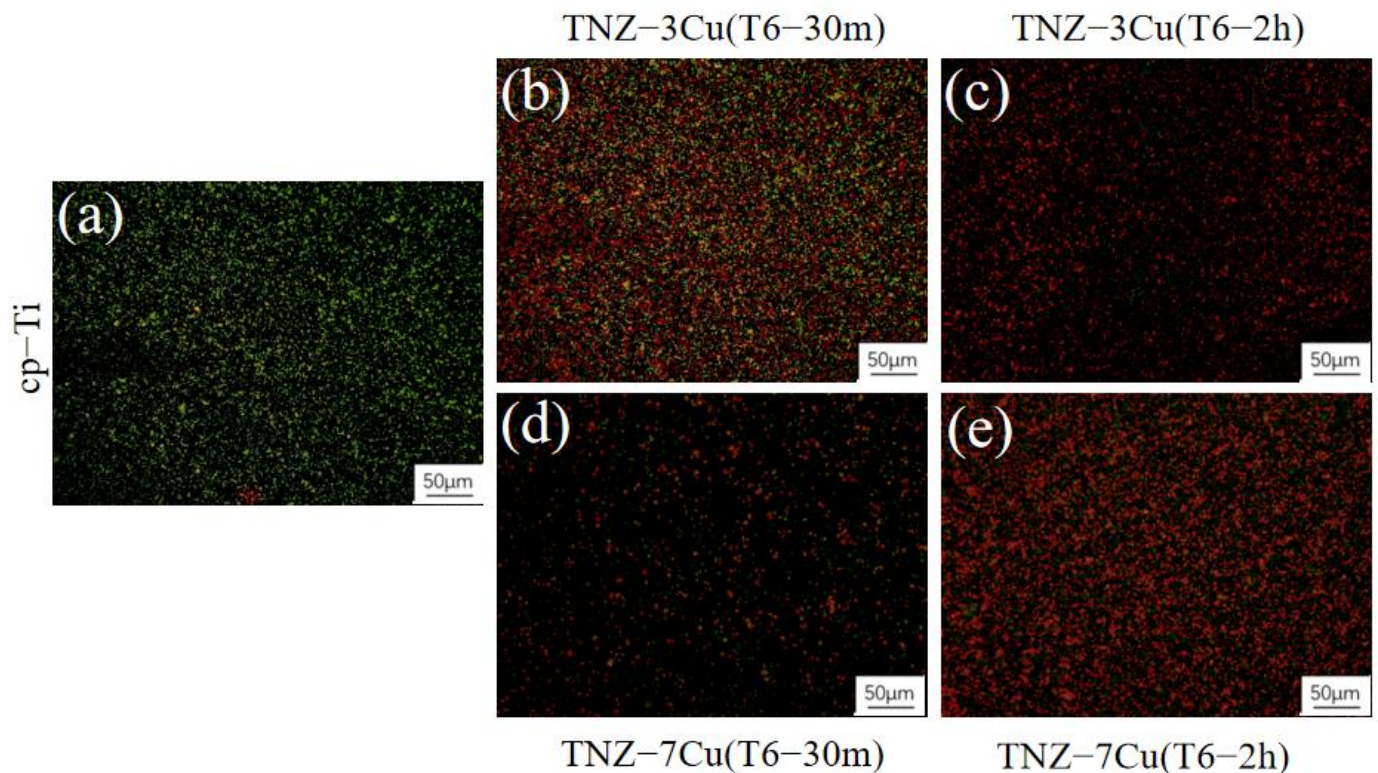


**Figure 11.** Live/Dead staining of *S. aureus* inoculated on the different samples for 24 h. (a) cp-Ti; (b) TNZ-3Cu(T6-30m); (c) TNZ-3Cu(T6-2h); (d) TNZ-7Cu(T6-30m); (e) TNZ-7Cu(T6-2h).

Figure 12 shows representative SEM micrographs of *S. aureus* inoculation for 24 h. As shown in Figure 12(a1,a2), a large amount of bacteria in completely spherical shape gathered on the surface of cp-Ti samples, indicating that the vast majority of *S. aureus* grew well. While on the surface of TNZ-3Cu(T6-2h) and TNZ-7Cu(T6-2h) samples, the number of bacteria decreased significantly, and the morphology of bacteria became irregular and began to sag, dry and adhere to each other, indicating the bacterial was killed or in a very bad condition.

### 3.7. Cell Cytotoxicity

Figure 13a shows the OD values of MC3T3-E1 cells co-cultured with the extracts of TNZ-3Cu(T6), TNZ-7Cu(T6), and cp-Ti samples for 1, 3, and 7 days. It can be found that the OD values of all extracts increased significantly with the extension of the culture time, indicating that the cells proliferated and grew well in the extracts. Although the OD values of TNZ-xCu groups were slightly higher than that of cp-Ti group, no significant difference in the OD value between the cp-Ti and TNZ-xCu (wt.%, x = 3, 7) group and among TNZ-xCu (wt.%, x = 3, 7) groups was found ( $p > 0.05$ ). Figure 13b shows the calculated cell viability. Compared with cp-Ti sample, all TNZ-xCu samples exhibited >100% viability. The above results demonstrated TNZ-xCu samples did not have cytotoxicity to MC3T3 cell line.

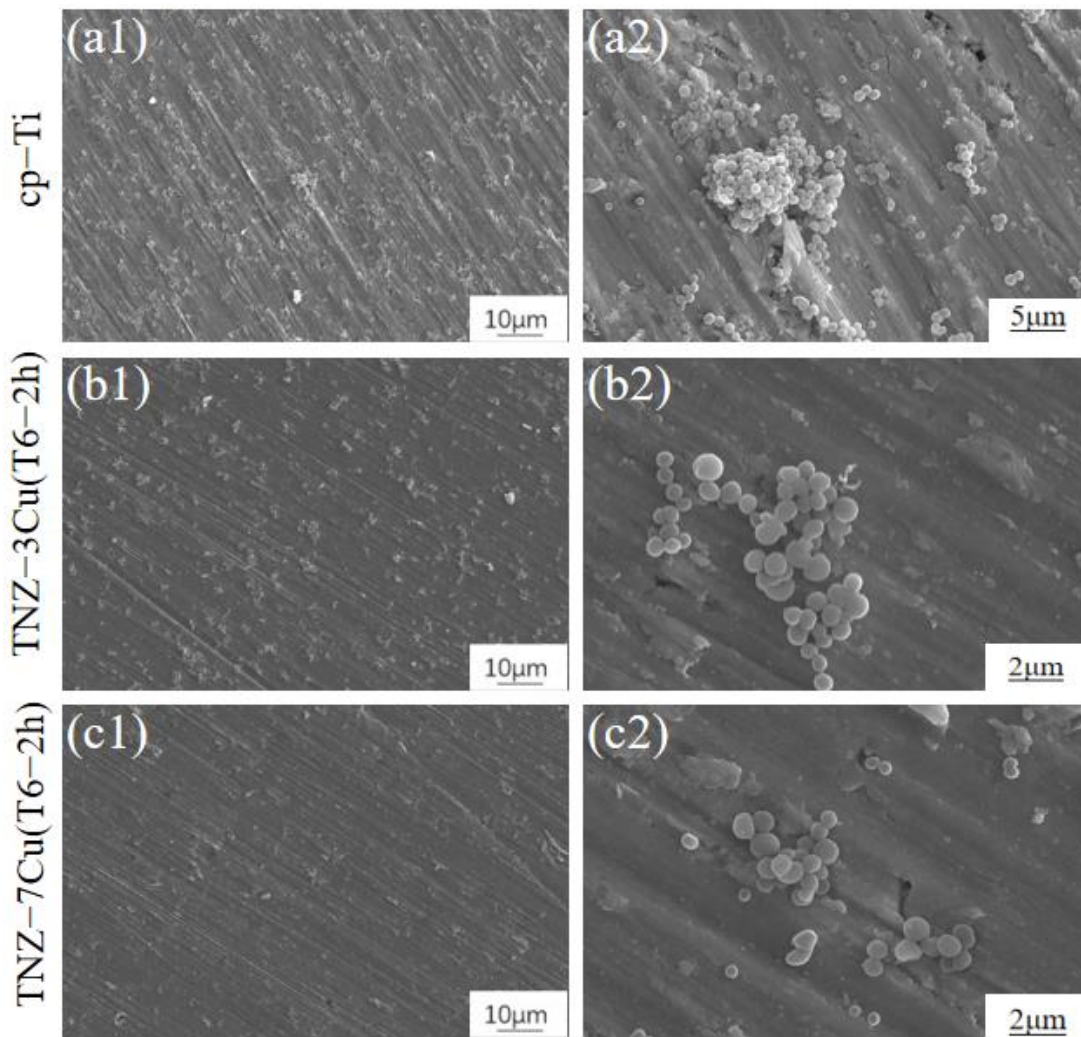


Figure 12. Morphology of *S. aureus* cultured on the samples surface for 24 h. (a1,a2) cp-Ti; (b1,b2) TNZ-3Cu(T6-2h); (c1,c2) TNZ-7Cu(T6-2h).

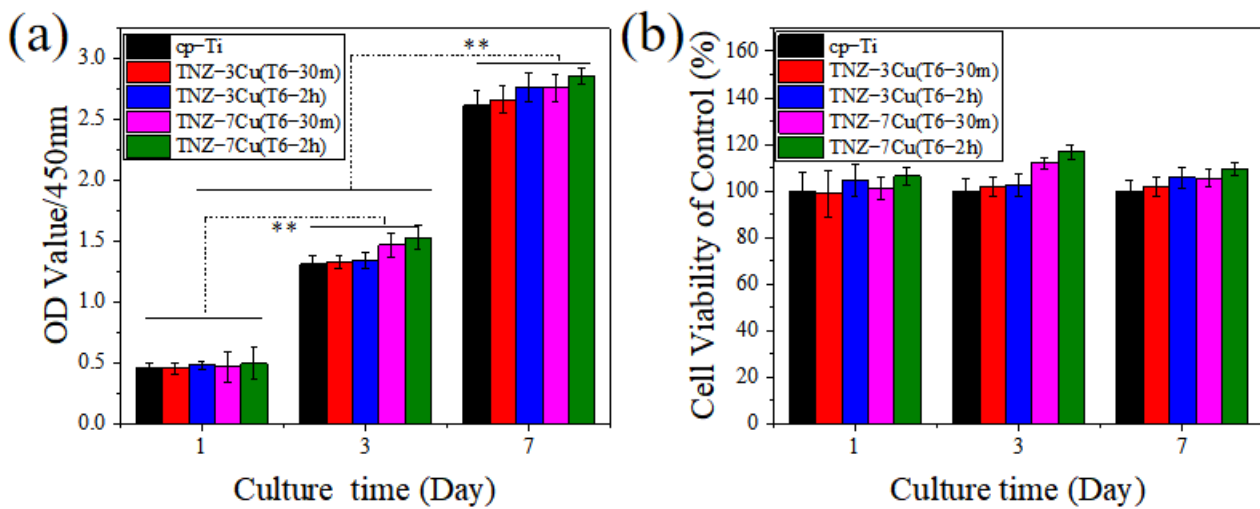
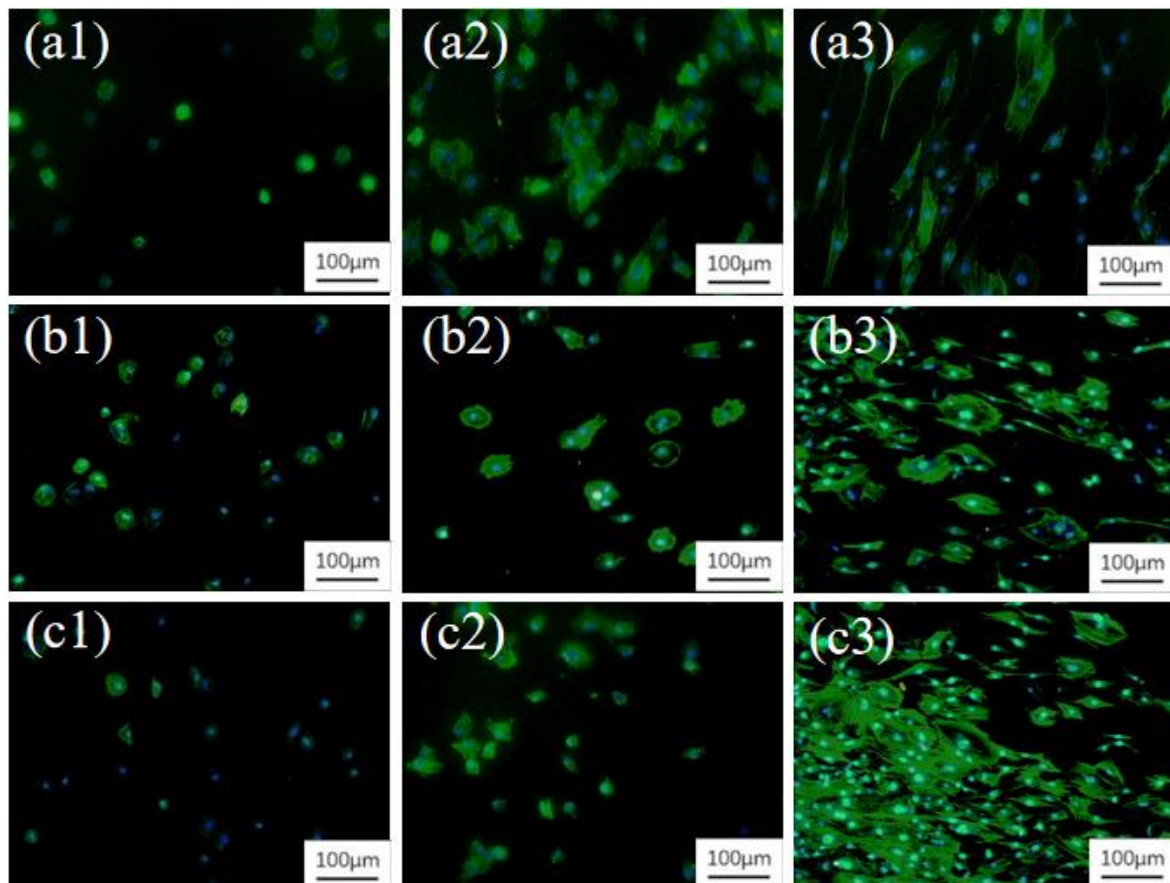


Figure 13. OD value and viability of MC3T3-E1 cells co-cultured with different sample extracts after 1-7 days (\*\*  $p < 0.05$ ): (a) OD value at 450 nm, (b) Cell viability.

### 3.8. Cell Adhesion Property

In this experiment, Dapi staining was applied to observe the adhesion and spread behavior of MC3T3 cells on the sample surface. Figure 14 shows the cells cytoskeleton on TNZ-xCu(T6-2h) and cp-Ti for 1 h, 4 h, and 24 h. The green fluorescent regions represent the cytoplasmic regions and the blue fluorescent regions represent the nuclear regions. At 1 h, some cells were in round shape in a single state on all surface. After 4 h incubation, the cells began to spread around and some cells fused together. As the incubation time extended to 24 h, large amount of the cells spread evenly all over the samples. The results showed that the cell had good adhesion property to all samples.



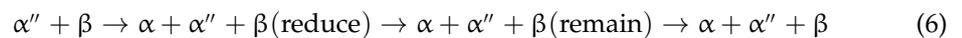
**Figure 14.** Cytoskeleton of MC3T3 cell on cp-Ti and TNZ-xCu (T6-2h) samples for 1 h, 4 h, and 24 h. (a1) cp-Ti for 1 h; (a2) cp-Ti for 4 h; (a3) cp-Ti for 24 h; (b1) TNZ-3Cu(T6-2h) for 1 h; (b2) TNZ-3Cu(T6-2h) for 4 h; (b3) TNZ-3Cu(T6-2h) for 24 h; (c1) TNZ-7Cu(T6-2h) for 1 h; (c2) TNZ-7Cu(T6-2h) for 4 h; (c3) TNZ-7Cu(T6-2h) for 24 h.

## 4. Discussion

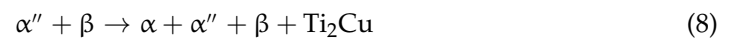
### 4.1. Phase Transformation

Some researchers have proved the addition of different content of copper in Ti-Cu alloy can effectively affect the microstructure of the alloy [19]. With the copper content increased, the phase composition gradually changed from a single  $\alpha''$  martensite phase to the complete  $\beta$  phase. In this study, a mixture of  $\alpha'' + \beta$  with the acicular  $\alpha''$  phase at the  $\beta$  phase boundary was found in both TNZ-3Cu(T4) and TNZ-7Cu(T4) samples. Even after short-term aging treatment, the  $\beta$  phase still occupied the majority of the alloy phase constitution, which indicates that Cu element has strong  $\beta$  phase stability.

In the TNZ-3Cu sample, the aging treatment accelerated the phase transformation process:



But  $\text{Ti}_2\text{Cu}$  phase precipitated from matrix while  $\beta$  phase was stabilized after 2 h aging treatment through the following reaction:



On the contrary,  $\text{Ti}_2\text{Cu}$  appeared in TNZ-7Cu(T6-15min), indicating that high Cu content promoted the precipitation of  $\text{Ti}_2\text{Cu}$  phase. In addition, high copper content led to high volume fraction of  $\text{Ti}_2\text{Cu}$ .

#### 4.2. Mechanical and Corrosion Properties

The hardness of an alloy is closely related to the hardness of each phase in the alloy as well as grain size. The hardness relationship of various phases in the TNZ-Cu alloy is in the following order:  $\text{Ti}_2\text{Cu} > \alpha' > \alpha'' > \alpha > \beta$ . According to the microstructure analysis in the above section, the T4 treated alloys were mainly composed of large amounts of  $\beta$  and small amounts of  $\alpha''$  phase, so the hardness of the alloys at T4 state was very low. As the aging process went on, the  $\alpha''$  phase was gradually transformed into  $\alpha$  phase, and  $\text{Ti}_2\text{Cu}$  phase with high hardness gradually precipitated. Therefore, the hardness of TNZ-xCu gradually increased with the extension of the aging treatment. The higher the copper content is, the more  $\text{Ti}_2\text{Cu}$  phase is. Therefore, the hardness of TNZ-7Cu was significantly higher than that of TNZ-3Cu at all intervals.

The elastic modulus of titanium alloy is primarily controlled by the phase constitution [20]. The elastic modulus of the phases from high to low is in the following order:  $E_{\text{Ti}_2\text{Cu}} > E_{\alpha} > E_{\alpha'} > E_{\alpha''} > E_{\beta}$ , therefore, TNZ-xCu(T4) alloy had a low elastic modulus, as shown in Figures 5 and 6. But it was still found that TNZ-7Cu(T4) alloy exhibited a higher elastic modulus than TNZ base alloy because of the presence of  $\alpha''$  phase. With the extension of the aging duration,  $\beta$  phase and  $\alpha''$  phase were transformed into  $\alpha$  phase and  $\text{Ti}_2\text{Cu}$  phase, so the elastic modulus of TNZ-xCu(T6) alloy increased, and higher than that of TNZ-xCu(T4) alloy. As a fast eutectoid alloying element, the high copper content will result in high fraction of  $\text{Ti}_2\text{Cu}$  phase. Thus, TNZ-7Cu alloy has a high elastic modulus than TNZ-3Cu.

Titanium alloy has excellent corrosion resistance to body fluids [21]. Ti-13Nb-13Zr has a self-corrosive current density of  $5 \times 10^{-7}$  A/cm<sup>2</sup>, similar to that of other implanted titanium alloys in Ringer's solution [22]. The researchers proved the presence of copper has an impact on the corrosion resistance of titanium alloy [23]; the corrosion resistance of titanium alloy can be improved by the precipitation of copper in the form of nano-scale  $\text{Ti}_2\text{Cu}$  phase from the matrix [24,25]. The microstructure result has showed copper was mostly dissolved in the matrix of TNZ-xCu(T4), and the electrode potential of copper was higher than that of titanium, so the electrode potential of the whole alloy was increased. As a result, there was nearly no difference in  $E_{\text{corr}}$  between TNZ-xCu(T4) alloys and cp-Ti, but TNZ-xCu(T4) alloys had a slightly lower  $i_{\text{corr}}$  than cp-Ti, as listed in Table 2.

With the extension of the aging treatment,  $\text{Ti}_2\text{Cu}$  precipitated gradually from the matrix, and the volume fraction increased with the extension of the aging treatment and the increase in Cu content, which caused the galvanic corrosion between  $\text{Ti}_2\text{Cu}$  and the matrix and fast corrosion as a result. However, TNZ-3Cu(T6) samples still exhibited the same  $i_{\text{corr}}$  as TNZ-3Cu(T4), suggesting the volume fraction of  $\text{Ti}_2\text{Cu}$  in TNZ-3Cu(T6) sample was high enough. The TNZ-7Cu(T6) samples showed a much higher  $i_{\text{corr}}$  than both TNZ-7Cu(T4) and cp-Ti, a high order of magnitude, revealing the negative effect of  $\text{Ti}_2\text{Cu}$  phase on

the corrosion resistance of the alloy. However, it must be noted that the corrosion rate of TNZ-xCu(T6) alloy was still very low.

Good corrosion resistance is a basic requirement of titanium alloy as a biomedical titanium alloy. Figure 15a summarizes the reported self-corrosion current density of several titanium alloys in simulated body fluid against the elastic modulus [10,11,26–28]. It can be concluded that TNZ-3Cu(T6) exhibited the lowest corrosion density and a low modulus among all these reported titanium alloys. On the other hand, Ti-13Nb-13Zr-10Cu prepared by powder metallurgy showed a much lower modulus, but a very high corrosion density.

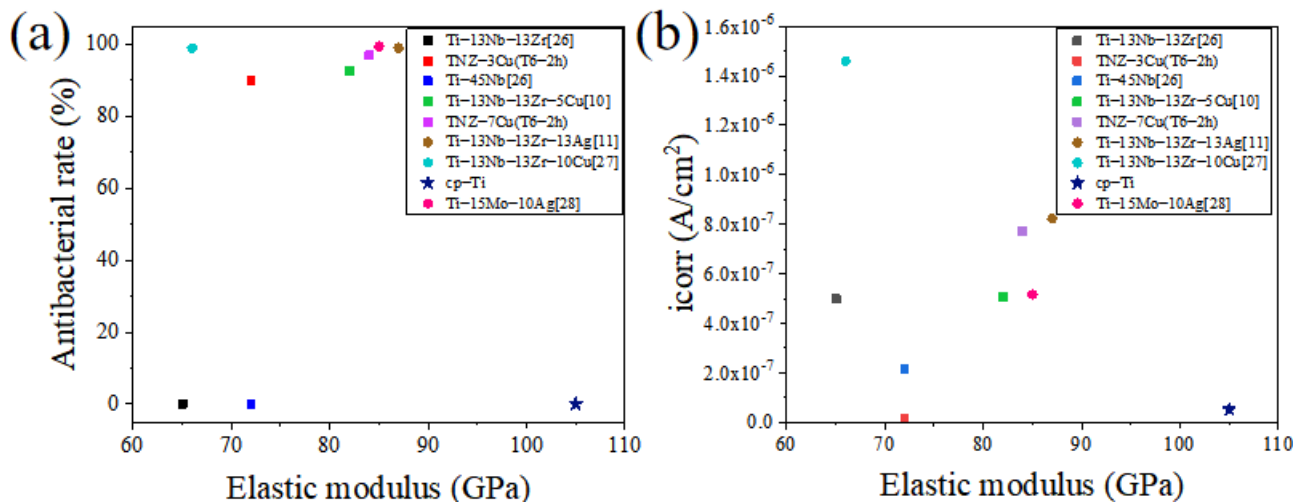


**Figure 15.** The result diagrams of elastic modulus, antibacterial effect, and self-corrosion current density ( $i_{corr}$ ) between titanium alloys: (a) The elastic modulus and antibacterial results of the titanium alloys, (b) the elastic modulus and self-corrosion current density results of the titanium alloys.

#### 4.3. Antibacterial Properties

So far, there are two main antibacterial mechanisms of Cu containing antibacterial titanium alloy [29,30]: one is that free Cu ions released from Ti-Cu alloy play an antibacterial role [31], and the other is that Cu-rich phase including Ti<sub>2</sub>Cu intermetallic compounds plays an antibacterial role due to the micro-area potential difference [6,32,33]. Some researchers have confirmed the Cu<sup>2+</sup> release concentration of Ti-Cu alloy must be (0.69–0.83) ppm to ensure good and stable antibacterial action [34]. Luethen confirmed the concentrations of copper ion in the (0.3–1.75) ppm range was effective in killing bacteria [31]. The maximum copper ion release concentration from TNZ-3Cu(T6-2h) and TNZ-7Cu(T6-2h) in the antibacterial test would be about 32.18 ppb and 71.63 ppb, far below the critical Cu<sup>2+</sup> concentration, which suggests that the antibacterial effect should be mostly controlled by the precipitation of Ti<sub>2</sub>Cu phase.

After T4 treatment, Cu mainly dissolved in the matrix, and very little Ti<sub>2</sub>Cu was formed in the alloy; therefore, no antibacterial property was detected on TNZ-xCu(T4) alloys. With the extension of the aging treatment, more Ti<sub>2</sub>Cu precipitated from the matrix as discussed in the above section. As a result, the antibacterial effect was enhanced with the extension of the aging times, as shown in Figure 10. Meanwhile, more Ti<sub>2</sub>Cu phases were found in the TNZ-7Cu samples than in the TNZ-3Cu sample; therefore, the TNZ-7Cu samples exhibited a higher antibacterial property than the TNZ-3Cu samples at all intervals. All these results confirm that the function of Ti<sub>2</sub>Cu phase is the important reason for the strong antibacterial effect of TNZ-xCu(T6) [25,35].

However, on the one hand, more Ti<sub>2</sub>Cu phase would result in a high elastic modulus. Therefore, it is of great significance to balance the elastic modulus and the antibacterial properties by reasonably selecting Cu content and microstructure controlling. Figure 15b shows the elastic modulus of titanium alloys and the antibacterial rate of the alloy against

*S. aureus*. Ti-13Nb-13Zr-10Cu [27], TNZ-3Cu, TNZ-5Cu [10], TNZ-7Cu, Ti-15Mo-10Ag [28] and Ti-13Nb-13Zr-13Ag [11] alloys all have low elastic modulus and good antibacterial effect. However, with the consideration of corrosion resistance in Figure 15b, TNZ-3Cu exhibited good comprehensive properties: low elastic modulus, very good corrosion resistance, and acceptable antibacterial property.

#### 4.4. Biocompatibility

Cu is an essential micronutrient and a cofactor of several enzymes that can build bone and promote angiogenesis [9,36]. However, excessive amounts of copper can be very harmful to the people's health, causing upset stomach and diarrhea [9]. The cytotoxicity of copper ion depends on concentration and cell line [6,37]. Concentrations of copper ion <8.5 mg/L are considered safe for many cell lines.

As shown in Figure 9b, the release of Cu ions in the TNZ-7Cu(T6-2h) and the TNZ-3Cu(T6-2h) samples was as high as 5  $\mu\text{g}/\text{L}/\text{cm}^2/\text{day}$  and 7  $\mu\text{g}/\text{L}/\text{cm}^2/\text{day}$  in the first 24 h, respectively. However, in Figure 13a, OD values of all samples are higher than cp-Ti, indicating that Cu ion release did not cause cytotoxicity. The morphology observation of MC3T3 on TNZ-xCu alloy and cp-Ti alloy in Figure 14 also confirmed that all cells began to adhere to each other through filamentous pseudopodia, and even some cells have begun to wrap each other through plasmodesmata, showing a state of mutual fusion. This further indicated that cells had good adhesion properties on each sample surface, which was conducive to cell spreading. However, it was reported that a small amount Cu ion release might promote cell proliferation and have a significant effect in reducing the formation of thrombus [9,31,38].

TNZ-xCu(T6) alloy has no cytotoxicity; it can slightly promote cell proliferation with the increase of copper ion leaching, and it has good biocompatibility. This shows that the use of TNZ-xCu (wt.%,  $x = 3, 7$ ) alloys can effectively reduce "stress shielding" and device-associated infections without any cytotoxicity. It is of great significance to further study the possible effects of Cu ion release on cell biological characteristics in TNZ-xCu samples. This research may provide new ideas for the development of biomedical titanium alloys, especially bone implants.

It has to be pointed out that there was no significant difference in the number and morphology of adherent cells between cp-Ti and TNZ-xCu(T6) samples and among TNZ-xCu(T6) samples, indicating that  $\text{Ti}_2\text{Cu}$  phase and Cu ion release did not affect cell adhesion and diffusion on sample surface. On the other hand, compared with cp-Ti samples, the presence of  $\text{Ti}_2\text{Cu}$  phase and the release of Cu ions did not improve cell adhesion, suggesting that it is necessary to conduct material surface modification to improve cell adhesion in future experiments, such as anodic oxidation [39] or plasma-based surface modification.

In view of the above results and discussion, TNZ-3Cu has lower elastic modulus, good biocompatibility, good antibacterial ability, and excellent corrosion resistance, which makes it a more ideal biomedical titanium alloy.

## 5. Conclusions

A new titanium alloy with low modulus and good antibacterial ability was designed and prepared by alloying Ti-13Nb-13Zr by Cu element followed by proper heat treatment. The results have demonstrated that the elastic modulus and the antibacterial properties increased significantly, but the corrosion resistance decreased slightly with the increase of Cu content and the precipitation of  $\text{Ti}_2\text{Cu}$ . The addition of Cu and the precipitation of  $\text{Ti}_2\text{Cu}$  phase did not affect the cytotoxicity of titanium alloys. Ti-13Nb-13Zr-3Cu with a low modulus of 73GPa, an antibacterial rate of over 90% against *S. aureus*, and good cell toxicity exhibited great potential as a candidate for implant titanium in the future. This paper provides a roadmap for the design and preparation of antibacterial and low-modulus titanium alloy in the future.

**Author Contributions:** Conceptualization, E.Z. and D.C.; methodology, X.M. E.Z. and D.C.; software, X.M. A.S. and R.W.; validation, X.M. E.Z. and D.C.; formal analysis, X.M. A.S. J.N. and G.Q.; investigation, X.M. A.S. R.W. and J.N.; resources, G.Q. E.Z. and D.C.; data curation, X.M. A.S. R.W. and J.N.; writing—original draft preparation, X.M.; writing—review and editing, E.Z.; visualization, D.C.; supervision, E.Z. and D.C.; project administration, G.Q.; funding acquisition, E.Z. All authors have read and agreed to the published version of the manuscript.

**Funding:** This research was funded by the National Nature Science Foundation of China (No.31971253, 51973.21), Beijing Municipal Health Commission (Grant No. BMHC-2021-6, BMHC-2019-9, PXM2020-026275-000002).

**Institutional Review Board Statement:** Not applicable.

**Informed Consent Statement:** Not applicable.

**Data Availability Statement:** Data sharing is not applicable.

**Conflicts of Interest:** The authors declare no conflict of interest.

## References

1. Niinomi, M. Titanium Alloys. In *Encyclopedia of Biomedical Engineering*; Narayan, R., Ed.; Elsevier: Oxford, UK, 2019; pp. 213–224.
2. Gerić, M.; Gajski, G.; Mihaljević, B.; Miljanić, S.; Domijan, A.-M.; Garaj-Vrhovac, V. Radioprotective properties of food colorant sodium copper chlorophyllin on human peripheral blood cells in vitro. *Mutat. Res. Genet. Toxicol. Environ. Mutagenesis* **2019**, *845*, 403027. [[CrossRef](#)] [[PubMed](#)]
3. Xu, D.; Lu, Z.; Wang, T.; Wang, S.; Jiang, Y.; Xu, Z.; Bi, Z.; Geng, S. Novel Ti-based alloys prepared with different heat treatment strategies as antibacterial biomedical implants. *Mater. Des.* **2012**, *205*, 109756. [[CrossRef](#)]
4. Baptista, C.A.R.P.; Schneider, S.G.; Taddei, E.B.; da Silva, H.M. Fatigue behavior of arc melted Ti–13Nb–13Zr alloy. *Int. J. Fatigue* **2004**, *26*, 967–973. [[CrossRef](#)]
5. Kuroda, D.; Niinomi, M.; Morinaga, M.; Kato, Y.; Yashiro, T. Design and mechanical properties of new  $\beta$  type titanium alloys for implant materials. *Mater. Sci. Eng. A* **1998**, *243*, 244–249. [[CrossRef](#)]
6. Zhang, Y.; Cui, S.; Cao, S.; Yang, L.; Qin, G.; Zhang, E. To improve the angiogenesis of endothelial cells on Ti-Cu alloy by the synergistic effects of Cu ions release and surface nanostructure. *Surf. Coat. Technol.* **2022**, *433*, 128116. [[CrossRef](#)]
7. Shirai, T.; Watanabe, K.; Matsubara, H.; Nomura, I.; Fujiwara, H.; Arai, Y.; Ikoma, K.; Terauchi, R.; Kubo, T.; Tsuchiya, H. Prevention of pin tract infection with iodine-supported titanium pins. *J. Orthop. Sci.* **2014**, *19*, 598–602. [[CrossRef](#)]
8. Ren, L.; Ma, Z.; Li, M.; Zhang, Y.; Liu, W.; Liao, Z.; Yang, K. Antibacterial Properties of Ti–6Al–4V–xCu Alloys. *J. Mater. Sci. Technol.* **2014**, *30*, 699–705. [[CrossRef](#)]
9. Zhang, E.; Zheng, L.; Liu, J.; Bai, B.; Liu, C. Influence of Cu content on the cell biocompatibility of Ti–Cu sintered alloys. *Mater. Sci. Eng. C* **2015**, *46*, 148–157. [[CrossRef](#)]
10. Shi, A.; Cai, D.; Hu, J.; Zhao, X.; Qin, G.; Han, Y.; Zhang, E. Development of a low elastic modulus and antibacterial Ti-13Nb-13Zr-5Cu titanium alloy by microstructure controlling. *Mater. Sci. Eng. C* **2021**, *126*, 112116. [[CrossRef](#)]
11. Cai, D.; Zhao, X.; Yang, L.; Wang, R.; Qin, G.; Chen, D.-F.; Zhang, E. A novel biomedical titanium alloy with high antibacterial property and low elastic modulus. *J. Mater. Sci. Technol.* **2021**, *81*, 13–25. [[CrossRef](#)]
12. Javadhesari, S.M.; Alipour, S.; Akbarpour, M.R. Biocompatibility, osseointegration, antibacterial and mechanical properties of nanocrystalline Ti-Cu alloy as a new orthopedic material. *Colloids Surf. B Biointerfaces* **2020**, *189*, 110889. [[CrossRef](#)] [[PubMed](#)]
13. Duan, R.; Li, S.; Cai, B.; Zhu, W.; Ren, F.; Attallah, M.M. A high strength and low modulus metastable  $\beta$  Ti-12Mo-6Zr-2Fe alloy fabricated by laser powder bed fusion in-situ alloying. *Addit. Manuf.* **2021**, *37*, 101708. [[CrossRef](#)]
14. Gerhard, W.; Boyer, R.R.; Collings, E.W. *Materials Properties Handbook: Titanium Alloys*. ASM International: Novelt, OH, USA, 1994.
15. Zhang, W.; Zhang, S.; Liu, H.; Ren, L.; Wang, Q.; Zhang, Y. Effects of surface roughening on antibacterial and osteogenic properties of Ti-Cu alloys with different Cu contents. *J. Mater. Sci. Technol.* **2021**, *88*, 158–167. [[CrossRef](#)]
16. Bao, M.; Liu, Y.; Wang, X.; Yang, L.; Li, S.; Ren, J.; Qin, G.; Zhang, E. Optimization of mechanical properties, biocorrosion properties and antibacterial properties of wrought Ti-3Cu alloy by heat treatment. *Bioact. Mater.* **2018**, *3*, 28–38. [[CrossRef](#)] [[PubMed](#)]
17. Xi, T.; Shahzad, M.B.; Xu, D.; Zhao, J.; Yang, C.; Qi, M.; Yang, K. Copper precipitation behavior and mechanical properties of Cu-bearing 316L austenitic stainless steel: A comprehensive cross-correlation study. *Mater. Sci. Eng. A* **2016**, *675*, 243–252. [[CrossRef](#)]
18. Thongsrikhem, N.; Taokaew, S.; Sriariyanun, M.; Kirdponpattara, S. Antibacterial activity in gelatin-bacterial cellulose composite film by thermally crosslinking with cinnamaldehyde towards food packaging application. *Food Packag. Shelf Life* **2022**, *31*, 100766. [[CrossRef](#)]
19. Sun, K.; Yi, X.; Sun, B.; Yin, X.; Meng, X.; Cai, W.; Zhao, L. Microstructure and mechanical properties of Ti–V–Al–Cu shape memory alloy by tailoring Cu content. *Mater. Sci. Eng. A* **2020**, *771*, 138641. [[CrossRef](#)]

20. Du, Z.; Guo, H.; Liu, J.; Cheng, J.; Zhao, X.; Wang, X.; Liu, F.; Cui, X. Microstructure evolution during aging heat treatment and its effects on tensile properties and dynamic Young's modulus of a biomedical  $\beta$  titanium alloy. *Mater. Sci. Eng. A* **2020**, *791*, 139677. [[CrossRef](#)]
21. Amigó-Borrás, V.; Lario-Femenía, J.; Amigó-Mata, A.; Vicente-Escuder, Á. Titanium, Titanium Alloys and Composites. In *Encyclopedia of Materials: Metals and Alloys*; Caballero, F.G., Ed.; Elsevier: Oxford, UK, 2022; pp. 179–199.
22. Kumar, P.; Mahobia, G.S.; Mandal, S.; Singh, V.; Chattopadhyay, K. Enhanced corrosion resistance of the surface modified Ti-13Nb-13Zr alloy by ultrasonic shot peening. *Corros. Sci.* **2021**, *189*, 109597. [[CrossRef](#)]
23. Jin, X.; Gao, L.; Liu, E.; Yu, F.; Shu, X.; Wang, H. Microstructure, corrosion and tribological and antibacterial properties of Ti-Cu coated stainless steel. *J. Mech. Behav. Biomed. Mater.* **2015**, *50*, 23–32. [[CrossRef](#)]
24. Chen, M.; Yang, L.; Zhang, L.; Han, Y.; Lu, Z.; Qin, G.; Zhang, E. Effect of nano/micro-Ag compound particles on the bio-corrosion, antibacterial properties and cell biocompatibility of Ti-Ag alloys. *Mater. Sci. Eng. C* **2017**, *75*, 906–917. [[CrossRef](#)]
25. Zhang, E.; Zhao, X.; Hu, J.; Wang, R.; Fu, S.; Qin, G. Antibacterial metals and alloys for potential biomedical implants. *Bioact. Mater.* **2021**, *6*, 2569–2612. [[CrossRef](#)] [[PubMed](#)]
26. Hu, N.; Xie, L.; Liao, Q.; Gao, A.; Zheng, Y.; Pan, H.; Tong, L.; Yang, D.; Gao, N.; Starink, M.J.; et al. A more defective substrate leads to a less defective passive layer: Enhancing the mechanical strength, corrosion resistance and anti-inflammatory response of the low-modulus Ti-45Nb alloy by grain refinement. *Acta Biomater.* **2021**, *126*, 524–536. [[CrossRef](#)] [[PubMed](#)]
27. Ke, Z.; Yi, C.; Zhang, L.; He, Z.; Tan, J.; Jiang, Y. Characterization of a new Ti-13Nb-13Zr-10Cu alloy with enhanced antibacterial activity for biomedical applications. *Mater. Lett.* **2019**, *253*, 335–338. [[CrossRef](#)]
28. Cui, S.; Liu, S.; Nie, J.; Chen, D.; Wu, X.; Qin, G.; Zhang, E. Design and preparation of a biomedical titanium alloy with low elastic modulus and high antibacterial property based on Ti-Mo-Ag system. *J. Alloys Compd.* **2022**, *908*, 164639. [[CrossRef](#)]
29. Burghardt, I.; Lüthen, F.; Prinz, C.; Kreikemeyer, B.; Zietz, C.; Neumann, H.-G.; Rychly, J. A dual function of copper in designing regenerative implants. *Biomaterials* **2015**, *44*, 36–44. [[CrossRef](#)]
30. Yang, J.; Qin, H.; Chai, Y.; Zhang, P.; Chen, Y.; Yang, K.; Qin, M.; Zhang, Y.; Xia, H.; Ren, L.; et al. Molecular mechanisms of osteogenesis and antibacterial activity of Cu-bearing Ti alloy in a bone defect model with infection in vivo. *J. Orthop. Transl.* **2021**, *27*, 77–89. [[CrossRef](#)]
31. Xia, C.; Ma, X.; Zhang, X.; Li, K.; Tan, J.; Qiao, Y.; Liu, X. Enhanced physicochemical and biological properties of C/Cu dual ions implanted medical titanium. *Bioact. Mater.* **2020**, *5*, 377–386. [[CrossRef](#)] [[PubMed](#)]
32. Fu, S.; Zhang, Y.; Yang, Y.; Liu, X.; Zhang, X.; Yang, L.; Xu, D.; Wang, F.; Qin, G.; Zhang, E. An antibacterial mechanism of titanium alloy based on micro-area potential difference induced reactive oxygen species. *J. Mater. Sci. Technol.* **2022**, *119*, 75–86. [[CrossRef](#)]
33. Lu, M.; Zhang, Z.; Zhang, J.; Wang, X.; Qin, G.; Zhang, E. Enhanced antibacterial activity of Ti-Cu alloy by selective acid etching. *Surf. Coat. Technol.* **2021**, *421*, 127478. [[CrossRef](#)]
34. Ren, L.; Xu, X.; Liu, H.; Yang, K.; Qi, X. Biocompatibility and Cu ions release kinetics of copper-bearing titanium alloys. *J. Mater. Sci. Technol.* **2021**, *95*, 237–248. [[CrossRef](#)]
35. Zhang, E.; Li, F.; Wang, H.; Liu, J.; Wang, C.; Li, M.; Yang, K. A new antibacterial titanium-copper sintered alloy: Preparation and antibacterial property. *Mater. Sci. Eng. C* **2013**, *33*, 4280–4287. [[CrossRef](#)] [[PubMed](#)]
36. Lucke, M.; Schmidmaier, G.; Sadoni, S.; Wildemann, B.; Schiller, R.; Haas, N.P.; Raschke, M. Gentamicin coating of metallic implants reduces implant-related osteomyelitis in rats. *Bone* **2003**, *32*, 521–531. [[CrossRef](#)]
37. Chen, M.; Wang, X.-Q.; Zhang, E.-L.; Wan, Y.-Z.; Hu, J. Antibacterial ability and biocompatibility of fluorinated titanium by plasma-based surface modification. *Rare Met.* **2022**, *41*, 689–699. [[CrossRef](#)]
38. Stigter, M.; Bezemer, J.; de Groot, K.; Layrolle, P. Incorporation of different antibiotics into carbonated hydroxyapatite coatings on titanium implants, release and antibiotic efficacy. *J. Control. Release* **2004**, *99*, 127–137. [[CrossRef](#)]
39. Cao, S.; Zhang, Z.-M.; Zhang, J.-Q.; Wang, R.-X.; Wang, X.-Y.; Yang, L.; Chen, D.-F.; Qin, G.-W.; Zhang, E.-L. Improvement in antibacterial ability and cell cytotoxicity of Ti-Cu alloy by anodic oxidation. *Rare Met.* **2022**, *41*, 594–609. [[CrossRef](#)]